Summer 8-17-2017

# A Novel Device for MR Foot Perfusion Stress Testing

David John Muccigrosso
*Washington University in St. Louis*

WASHINGTON UNIVERSITY IN ST. LOUIS

School of Engineering and Applied Science

Department of Biomedical Engineering

Thesis Examination Committee:
Jie Zheng, Chair
Mark Anastasio
Patricia Widder

# A Novel Device for MR Foot Perfusion Stress Testing

by

David John Muccigrosso

A thesis presented to the School of Engineering
of Washington University in St. Louis in partial fulfillment of the
requirements for the degree of
Master of Science in Biomedical Engineering

August 2017

St. Louis, Missouri

# Contents

# List of Figures

# List of Tables

# List of Abbreviations

| | |
|---|---|
| DAQ | Data Acquisition |
| GUI | Graphical User Interface |
| MVC | Maximum Vulnerable Contraction |
| TC | Calibration Time |
| CB | Calibrated Baseline |
| CM | Calibrated Maximum |
| TCM | Time until Calibrated Maximum |
| CEP | Calibrated Exerted Pressure |
| QC | Quality Calibration |
| TS | Total Scan time |
| TSS | Time until Stable Stress |
| TPSS | Time Post Stable Stress |
| %TiRPSS | Percent Time in Range Post Stable Stress |
| EPSS | Exerted Pressure during Stable Stress |
| MEPSS | Mean Exerted Pressure during Stable Stress |
| VEPSS | Variance of Exerted Pressure during Stable Stress |
| SSEEPSS | Sum of Squared Errors of Exerted Pressure during Stable Stress |
| TEP | Target Exerted Pressure |
| %VAR(SI) | Percent Variance of Signal Intensity |
| SMBF | Skeletal Muscle Blood Flow |
| T | Training scan |
| P1 | Perfusion (stress) scan 1 |
| P2 | Perfusion (stress) scan 2 |
| R1 | Rest scan 1 |
| R2 | Rest scan 2 |

# Acknowledgments

I would like to thank Jie Zheng for helping me build my career and motivating this research; all of my professors and advisors who got me through pre-med and grad school; Jasmine Park for helping me figure out how to work a sewing machine; Zack Marlow and Professor Ramesh Agarwal for their help on the leak modeling, Washington University for providing me this unique opportunity; my family – especially Mom, Dad, and Grandma – for all of the blessings they have given me throughout my life; my stepbrother Phil, for picking up the slack at home; and Beth for her patience, support, and for always demanding the best from me.

This research was funded by NIH grant 5R01DK105322

David Muccigrosso

*Washington University in St. Louis*

*August 2017*

For Beth.

ABSTRACT OF THE THESIS

A Novel Device for MR Foot Perfusion Stress Testing

by

David John Muccigrosso

Master of Science in Biomedical Engineering

School of Engineering Arts and Sciences

Washington University in St. Louis, 2017

Professor Jie Zheng, Chair

Foot ulcers are a serious complication of diabetes mellitus (DM). Perfusion impairment in muscles and bone below the ulcer strongly predicts wound healing, but no modalities can currently probe deeply enough into the foot to adequately assess perfusion. We developed and validated an MR-compatible device for quantitative, noninvasive regional perfusion measurement in the diabetic foot. We conducted an evaluation study with 4 control and 9 DM/ulcer patients, and developed statistical measures to quantify subject performance. Subjects successfully achieved consistent exertion during stress MR scans, as measured by a strong correlation between their mean exerted pressure and the target pressure. DM patients had significantly elevated skeletal muscle blood flow (SMBF) over controls, and higher exerted pressure variance from target. Areas of future improvement were identified. This device is a promising step towards clinical MR foot perfusion stress testing that may lead to improved diagnostics and treatment for diabetic foot ulcer diagnostics.

# 1. Background

## 1.1 OVERVIEW OF DIABETES MELLITUS

Diabetes mellitus (DM) is a progressive metabolic disease that is primarily characterized by two types - innate insulin deficiency (I) and acquired insulin resistance (II). It affected 29.1 million Americans in 2012, and there are 1.4 million new diagnoses annually; DM and its complications are the 7th leading cause of death as well [1]. Foot ulcerations are among the more serious complications of DM, and between 15-25% of DM patients will develop an ulcer or require a hospitalization because of one in the course of their disease [1, 2]. For the purposes of this study, we will focus on perfusion abnormalities in the ulcerated diabetic foot.

## 1.2 FOOT ULCERS

A foot ulcer is defined as a breakdown in the skin of the foot, which may extend into the subcutaneous tissue, bone, and even muscle. The prime contributors to ulcer formation and impaired ulcer healing in the diabetic foot are: neuropathy, biomechanical pressure, microtrauma, infection, immune cellular dysfunction and impaired regional perfusion. Impaired regional perfusion results in decreased delivery of oxygen, nutrients, and immune cells critical to wound bed healing [3, 4]. Impaired regional perfusion also contributes to diabetic neuropathy, which may play a reciprocal role by causing arteriolar constriction. The extension of the wound bed well into the dermis and muscles of the foot is evidence for the importance of skeletal muscle perfusion to ulcer formation [5]. In patients with DM, reduced capillary size and basement membrane thickening cause impaired resting perfusion and/or vasodilatory response to challenge [6]. Using intra-arterial injections of radioactive microspheres, it was found that ulcers

healed in 90% of patients with high lesion perfusion, versus only 10% of ulcers that healed in patients with low lesion perfusion [7]. In a study of 2511 diabetic foot ulcer patients, 48.8% were ischemic; amputation was associated with peripheral vascular disease (PVD) and ulcer type, but not age, sex, duration of diabetes, neuropathy, deformity, or duration of ulcer [4]. Importantly, ulcers are often associated with diffuse and/or distal capillary narrowing, rendering them unsuitable for revascularization surgery. This subset of patients may receive prolonged medical treatment with no guarantee of wound-healing success. If the disease escapes control and becomes life-threating, amputation is inevitable. Taking all of these studies together, a generalized model of the impact of regional perfusion on diabetic foot ulceration can be illustrated (Figure 1).

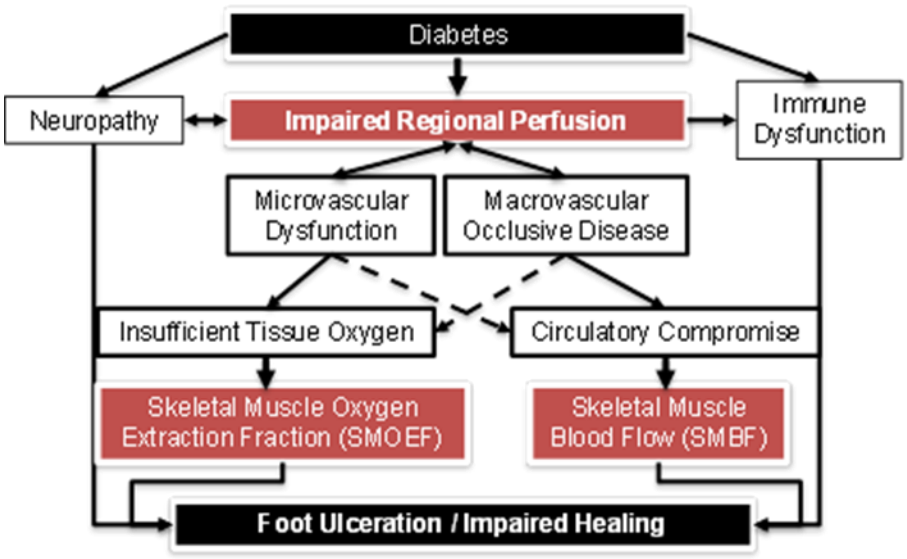


**Figure 1.** The central role of wound perfusion on the development and healing of pedal wounds in diabetics.

## 1.3 FOOT PERFUSION IMAGING OF THE MICROCIRCULATION

Macrocirculation in the peripheral vascular system can be measured using standard angiographic techniques (X-ray, CT, MR), but is not a complete measure of regional perfusion. Direct assessment of the microcirculation is a key to early detection of decreased perfusion in identifying patients with poor ulcer healing and high amputation risk. Traditionally, microcirculation is assessed using ankle/brachial index (ABI) or toe pressure [8], plethysmography [9, 10], capillaroscopy [11, 12], thermography [13], laser doppler flowmetry (LDF) [14], laser doppler Imaging (LDI) [15], transcutaneous oximetry ($TcPO_2$) [16], skin perfusion pressure [17], or orthogonal polarization spectral imaging [18]. Although these techniques (except toe pressure, which assesses microvasculature) assess either focal skin perfusion or oxygenation (< 3 mm depth), they have relatively low spatial resolution, reliability, and sensitivity, and provide little information on regional perfusion or oxygenation in deep skeletal muscle [19]. $TcPO_2$ has been used to assess skin perfusion and oxygenation in the diabetic foot for amputation level selection [20, 21]. A hyperspectral imaging technique was used to observe a decrease in oxyhemoglobin at ulceration sites, and an increase in oxyhemoglobin around the ulcer as it healed and closed [22]. However, these results are qualitative and greatly influenced by many factors that inhibit the transmission of oxygen, including obesity, subcutaneous inflammation, and swelling; and which are often seen in ulcerated diabetic feet. In a comparative study with control subjects, subjects with DM and foot ulcers, and subjects with DM and without foot ulcers, neither $TcPO_2$ nor microvascular hyperemic responses in the skin were able to discriminate between individuals with or without ulceration [23]. Conversely, it is reasonable to assume that the changes related specifically to

diabetes would be identifiable in muscle tissue. In an early study, an intra-arterial injection of $^{99m}$Tc-macroaggregated albumin was performed in patients with DM and foot ulcers [24]. This perfusion technique allowed evaluation of the whole capillary circulation in the foot. It was found that normal or increased perfusion muscle near the ulcer was significantly associated with successful healing (26/35 healed ulcers), whereas poor local muscle perfusion was always associated with non-healing ulcers (5/5 non-healed ulcers). However, this technique suffers from low spatial resolution, the use of radiation, and invasive intra-arterial injection. Using a high-resolution $^{31}$P-MR spectroscopy technique [25], the Pi/PCr ratio was observed to significantly increase in the metatarsal head muscle region in diabetic patients with and without neuropathy, versus normal controls. This result indicated reduced energy reserve and/or oxygen supply in the muscle of the diabetic foot. Taken together, these studies suggest that perfusion assessment of the bone and/or muscle tissue beneath the ulcer may be equally or more important in predicting ulcer healing than perfusion assessment of the boundary area around the wound bed.

## 1.4 OBJECTIVE

The ultimate goal of this research was to create more accurate methods than the current standard of care for the diagnosis and risk stratification of DM patients with foot ulcers. An MR perfusion test would allow for spatially localized, accurate, and noninvasive measurement of the ulcerative wound bed without ionizing radiation. The result would be an efficient and informed wound management plan that minimizes the patient and medical system burden. One strategy to assess whether tissue perfusion is adequate is to measure perfusion during the stress. This is because the rest perfusion value may not change for mild and moderate disease conditions, and

can be too small to measure accurately. Stress perfusion, on the other hand, can reveal perfusion impairment in damaged or diseased tissues.

In our previous work, we have developed MR methods for quantitative skeletal muscle blood flow (SMBF) mapping in calf, using arterial spin labeling (ASL) MR techniques [26, 27, 28, 29]. The stress in calf imaging was induced by isometric flexion of a foot on a pedal with specified resistance using a custom-made MRI compatible exercise system. Since foot perfusion stress testing is a special challenge due to the anatomy of the foot muscles, we set out to develop a method for inducing localized and non-pharmacological stress, while quantifying foot perfusion with our MR perfusion techniques.

# 2. Materials & Methods

## 2.1 Foot Perfusion Stress Device

The device had 4 components: 1) the foot assembly, 2) pneumatic pressure sensor, 3) digital gauge and DAQ, and 4) laptop, projector, and custom software.

The foot assembly was essentially a large housing of clear plastic boards for the subject's foot, the MR coil, and the sensor. It was produced by the Washington University School of Medicine's machine shop with input from Prof. Zheng, Professors from Physical Therapy (Professor Michael Mueller and Mary Hastings), and myself. Later redesigns used the Autodesk Inventor Student Edition to incorporate a number of ideas for improvement. The foot device consisted of a base, and an insert mounted with an adjustable sensor stage (Figure 2A). The

clearance between the insert and base was designed to ensure that the MR coil and sensor bulb could fit comfortably and stably around the foot to maximize RF reception. The stage had several axes of freedom to accommodate varying foot geometry. It featured a bar for the toes to curl around, ensuring that the correct muscle would be exercised.

The sensor was a rubber half-bulb (Figure 2B). The bulb was mated to a plastic tube and a coupler, with all joints sealed and tested for airtightness.

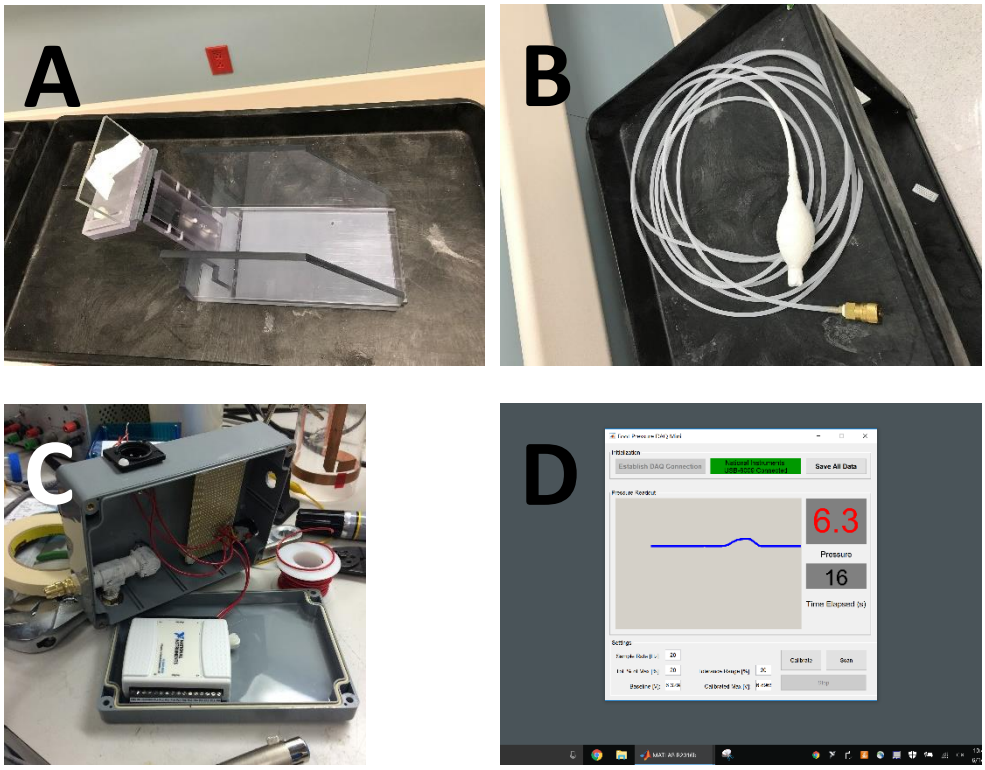


**Figure 2.** Photos of (A) foot assembly, (B) sensor bulb, (C) gauge and DAQ circuitry, and (D) feedback GUI interface.

The other end of the coupler was connected to an assembly of ¼’ brass pipe fittings to form a sealed system between the coupler, digital gauge, and air inlet valve. The number of

fittings was minimized to reduce possible leak points. An Ashcroft 2074 digital gauge was chosen for its analog output wiring capability. A simple circuit (Figure 3) was designed to convert its signal to within the input range of the DAQ, a National Instruments USB-6009. These components were enclosed in a circuitry box (Figure 2C).

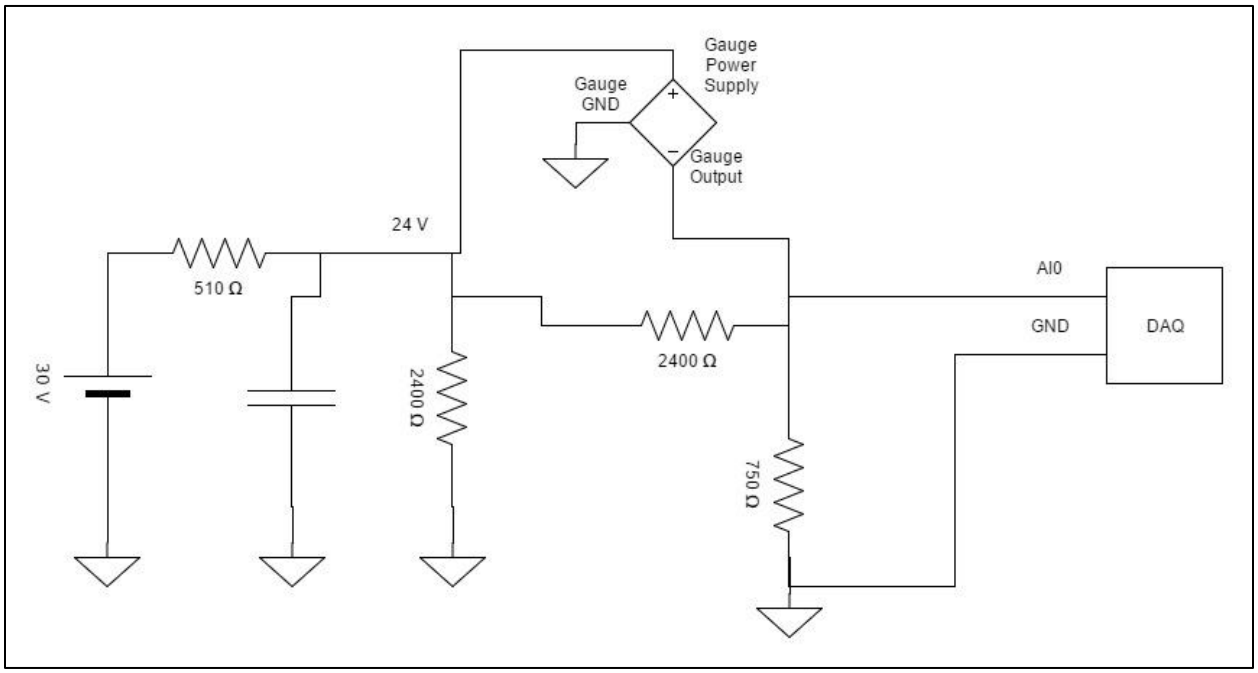


**Figure 3.** Circuit diagram for gauge and DAQ.

Finally, a custom GUI interface was developed in MATLAB to display the DAQ readout in real time (Figure 2D). This could be run on a laptop and projected onto the front panel of the MR scanner facing the subject. A sensory feedback display was designed for the subject so that the force level exerted in real time can be visualized so that the subject can adjust exertion force to maintain the force level within a defined range.

The voltage time series data was autosaved in a ".mat" and a ".xlsx" file after each acquisition. A 5-pole median averaging filter step was used to smooth out the raw voltage curve to prevent system noise from creating a positive feedback loop with the subject – like an airline pilot overcorrecting previous inputs in reaction to a single perturbation. The two main acquisition modes were already mentioned: "calibration" and "scan". Calibration mode calculated a baseline voltage from the average of the first five seconds, and then used a max value to determine the maximal contraction force or maximal vulnerable contraction (MVC) (Figure 4A). Scan mode presented a force range displayed with two red dashed lines at a specified fraction above and below a percentage of the calibrated max (Figure 4B). These percentages were adjustable, but were each set at 20% for the entirety of this study, i.e., at 20% MVC. The sampling rate was also adjustable; originally scans were sampled at 5 Hz, but this was later increased in to 20 Hz to reduce the delay induced by the median averaging filter.

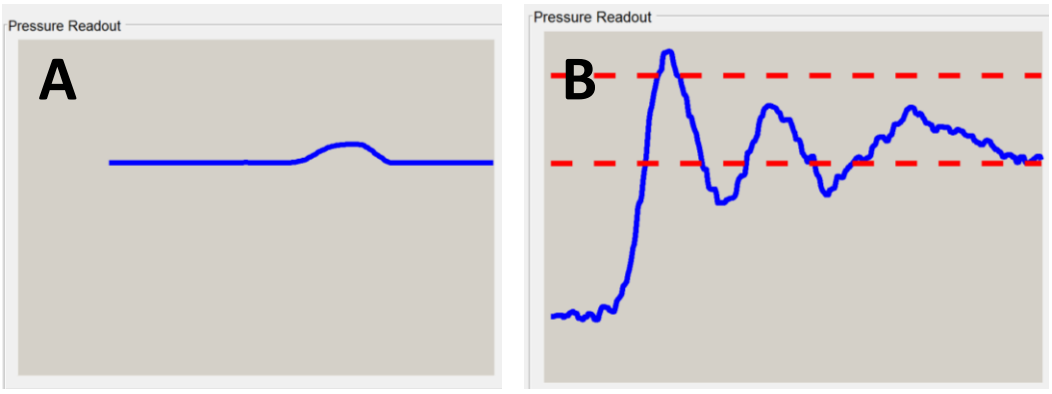


**Figure 4.** (A) Calibration mode. (B) Scan mode.

## 2.2 Study Design

The study consisted of two main elements: a validation experiment to ensure that the stress device was properly working, and an evaluation study in subjects using the stress device. In the validation experiment, two tests were performed. The first was leak testing to ensure that the pneumatic parts of the device were adequately sealed. The second test was to create a pressure-voltage curve between the pressures measured by the digital gauge and the voltages measured by the DAQ circuits. The pneumatic sensor bulb was pressurized to 4 psi, and then allowed to slowly deflate to 1 psi while acquiring voltage data in real time.

The evaluation study was approved by the Institutional Review Board at Washington University in Saint Louis. For the study, 13 subjects were recruited: 4 were healthy controls and the other 9 were DM patients with and without ulcers. All subjects were scanned on a Siemens Trio 3T system in the Center for Clinical Imaging Research of the Mallinckrodt Institute of Radiology at Washington University School of Medicine.

The study protocol consisted of a training stage, then scout and rest imaging for three slices (3 min), and finally the stress test portion (3 min).

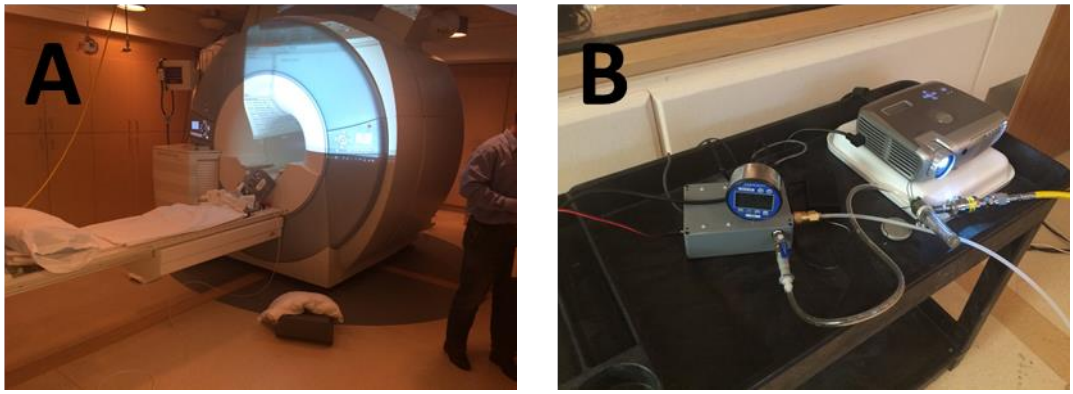


**Figure 5.** (A) Mock setup of the system. The subject lays their head on the pillow to the left, placing their foot in the apparatus at right. In the top center-right, the projector display can be seen. (B) The projector and device were set up as far away from the scanner as possible to minimize projectile risk. At center right, the scanner bay medical air hose (yellow) and regulator can be seen.

In the training stage, the subject was positioned supine with their foot in the foot device to conduct a mock version of the scan with only the device active (Figure 5). The pneumatic sensor was pressurized to between 2.5 and 3 psi. The pressure in the system was monitored such that if it fell below 1.5 psi, the system was repressurized. Padding was placed under the subject's foot for comfort. The device was calibrated by obtaining a 5 second baseline, and a maximal pressure on the sensor (Figure 6). A voltage increase above the baseline of 0.2 V was considered to be a "good" calibration - this will be discussed later in Discussion section. After maximal pressure, the subject was instructed to relax, and the acquisition was continued to ensure that the subject's exertion had not caused a leak in the system (which would be characterized by a subsequent drop well below the initial baseline). The subject then went through a training scan-mode acquisition, to familiarize them with the stress targeting software display. Once the subject achieved stable stress (SS) in the training scan, the study was proceeded.

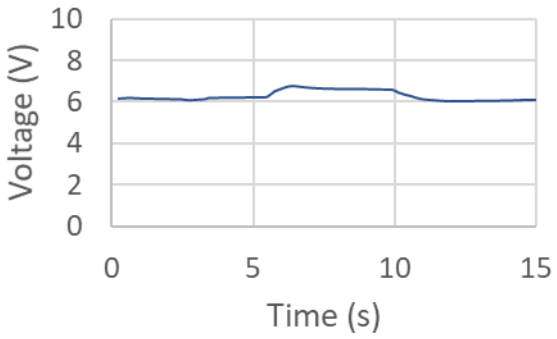


**Figure 6.** Diagram of calibration curve, scale slightly exaggerated for clarity.

The MR scan protocol began with traditional scout imaging and continued with rest perfusion imaging. The specific MR sequence used for the perfusion imaging was an ASL sequence that has been developed in our lab [28, 29]. Lastly, the stress imaging portion began with recalibrating the device (due to the system's intrinsic leak rate) and starting a new acquisition scan. The subject was instructed to keep the stress targeting software display within the range presented, and once they achieved SS for approximately 10-15 seconds, or if it appeared that their reaching SS was unlikely due to either technical complications or DM-related neurological deficit, the aforementioned MR protocol of perfusion imaging was begun. Afterwards, the subject was removed from the scanner, the device acquisitions were backed up, and the MR data was backed up. The MR scans were analyzed with custom software developed in our lab.

## 2.3 Raw Data Analysis

For the pressure-voltage curve, two sets of data were obtained. The DAQ was run in calibration mode starting at exactly 4.0 psi (read on the digital gauge) and allowed to leak until

exactly 1.0 psi, with no force exerted on the sensor. A smartphone (iPhone 7, iOS 10) stopwatch was run simultaneous to the DAQ scan, starting at exactly 4.0 psi with the time noted for every 0.1 psi of pressure lost. This gave a large set of paired voltage-time measurements. Since the pressure and voltage were recorded known at each time point on the stopwatch, a pressure-voltage curve could be calculated, along with a trendline and $R^2$ value.

The analysis of the evaluation study data was much more extensive. Several statistical measures were identified and calculated for the testing of various hypotheses (Figure 7). For calibrations, the measures included: calibration time (TC), calibrated baseline (CB), calibrated maximum (CM), time to calibrated maximum (TCM), calibrated exerted pressure (CEP), and quality calibration (QC). The calibrated exerted pressure was defined as CM - CB. A QC was defined as whether CEP exceeded 0.2, which as mentioned earlier was observed to be a practical predictor of subject performance.

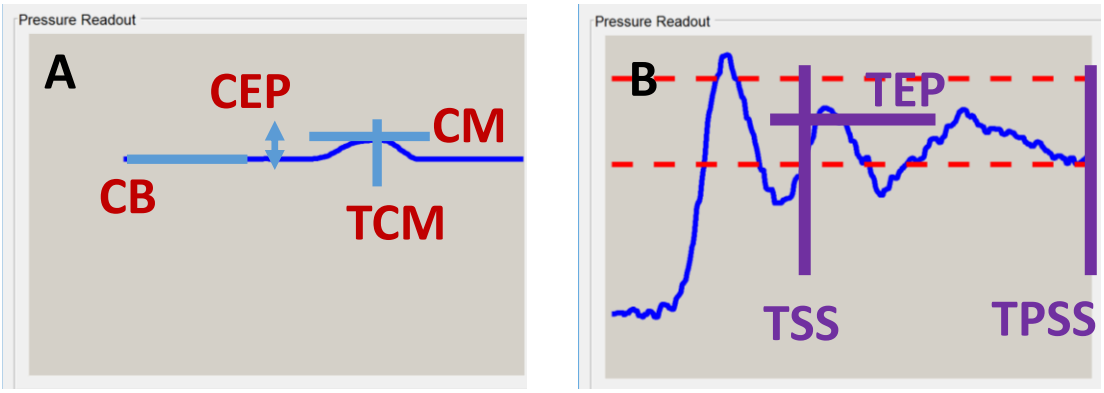


**Figure 7.** Diagram of selected statistical measures.

For scan mode, the measures included: the total scan time (TS), time until stable stress (TSS), time post stable stress (TPSS), percentage of time in range post stable stress (%TiRPSS), exerted pressure during stable stress (EPSS) and its mean (MEPSS), variance (VEPSS), and sum of squared errors (SSEEPSS), and target exerted pressure (TEP).

Lastly, the SMBF values were calculated using our custom-made perfusion mapping software, the ImPro MR Analysis Suite, written in MATLAB. Because a simple ROI (region of interest) variance measurement for each image would not have been meaningful, a composite measure had to be developed, %VAR(SI) (Figure 8). This was due to the nature of the 4-average ASL sequence used to acquire the MR images. Each set of 64 images was split into 4 averaging groups of 16, which were further divided into equal sets of 8 slice-selective and non-slice-selective frames. Each set of 8 images captured was a sample of a time point along a T1 recovery curve; thus, both the mean signal level and variance are constantly changing from frame to frame. Thus, the percent variance differences were calculated between each image in each set of 8 images and its corresponding other three averaging sets, and then averaged those eight values together to create a total of 6 sequential %VAR(SI) values. Since 3 slices were obtained for each 4-minute rest or perfusion scan, this led to a total of 18 %VAR(SI) values.

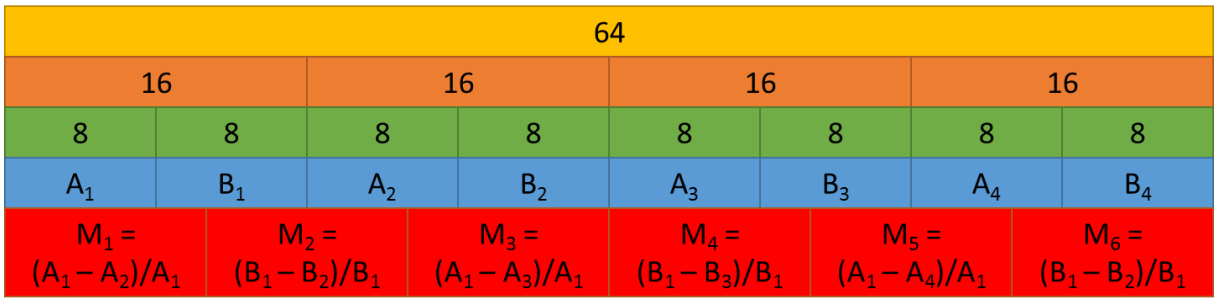

**Figure 8.** Breakdown of %VAR(SI) calculation, as represented by the M values at the bottom, for a single ASL slice.

## 2.4 Statistical Analysis

As mentioned, a number of hypothesis tests were done to answer specific questions about the relationships between each measure. These questions break down into three broad groups: training, performance, and perfusion. Unless stated otherwise, two-tailed Student's *t*-tests were performed for each hypothesis test, with homoscedasticity tested for each distribution based on its variance. For correlations, measures were plotted and regressed against each other, with $R^2$ values reported. Mean and standard deviations were calculated for all measures, but CM, CB, TC, and TS were omitted from the rest of the analysis because they were not inherently related to subject training or performance. The measures were grouped into three categories: calibration (CEP, QC, TCM), performance (TSS, %TiRPSS, VEPSS, SSEEPSS), and perfusion (%VAR(SI), SMBF).

For the training phase, we tested the hypothesis that there would be any significant differences between the control and DM (C/DM) groups during training (T) for the relevant measures – TC, CEP, and TSS. The same tests were run for the larger set of measures applicable to each perfusion group (P1/P2), including TC, CEP, and the performance measures.

In analyzing performance, we broadly sought to find (1) trends in performance, (2) correlations between calibrations and subsequent scan performance, and (3) links between training and performance. The first (1) was done by comparing the TSS differences for T/P1 and

P1/P2 (TSS was the only measure calculated for T), testing for significant differences for C/DM and P1/P2 with the other three performance measures (%TiRPSS, VEPSS, and SSEEPSS), and plotting and regressing the correlation between MEPSS and TEP. The second (2) was done by plotting and regressing P1/P2 calibration measures against the performance of the subsequent scan. For CEP vs. VEPSS and CEP vs. SSEEPSS, the intercepts were set to zero for both trendlines because linear regression would have predicted a negative intercept, which would not have been meaningful for these measures; this reduced the $R^2$ values as a result. For QC vs. %TiRPSS, VEPSS, and SSEEPSS, we tested for significant differences between the QC=TRUE and QC=FALSE sets within P1, P2, DM, and the global group (there were not enough QC=TRUE degrees of freedom for C). The third (3) was done by plotting and regressing T calibration measures against all P1/P2 calibration and performance measures. A special set of $\chi^2$-tests was performed for the T QC vs QC of the P1/P2, C/DM, and global sets. Again, no hypothesis tests could be done for C QC against any other measure.

For perfusion, we sought to (1) confirm perfusion elevation from the rest (R1/R2) to stress state, and (2) identify correlations between perfusion and performance measures. The first (1) was accomplished by testing for significant differences between R1/R2 and P1/P2 perfusion measures, and further broke these tests down into the global and C/DM sets. Additionally, we created a timewise boxplot of the absolute value of %VAR(SI) along its 18-point time course. For the second (2), we plotted and regressed P1/P2 perfusion measures against performance measures.

# 3. Results

There were 2 main results to report from this study: 1) the pressure-voltage curve, and 2) the evaluation study analysis. It is noted that the air-bubble leak testing during the device building process resulted in no visible leaks. Many results have been omitted due to lack of significance; this will be noted where relevant.

## 3.1 Pressure-Voltage Curve

The linear model equation, below, summarizes the correlation that was found between pressure and voltage (Figure 9), for which the $R^2$ value was 0.9998:

$$VOLTAGE = 0.2587\ (V/psi) \times PRESSURE + 5.6398\ (V) \qquad \textbf{Equation 1}$$

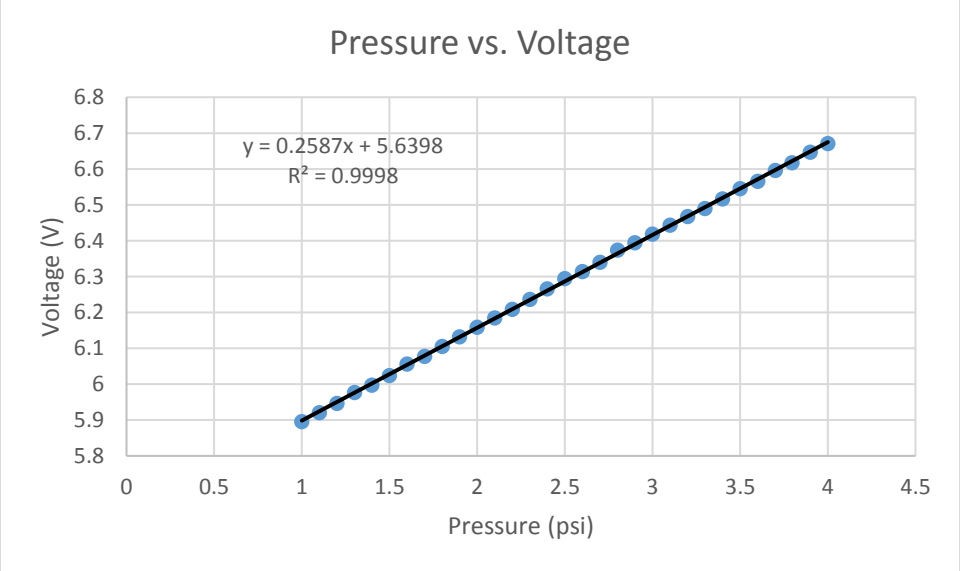


**Figure 9.** Pressure-voltage curve with trendline.

## 3.2 Evaluation Study

There were a total of n = 13 subjects. Table 1, below, gives a summary of the statistics that were calculated from our DAQ and MR data.

| n = 13 | T | P1 | P2 |
|---|---|---|---|
| **TC (s)** | 19.8 ± 9.10 | 21.2 ± 5.51 | 19.9 ± 3.38 |
| **CB (V)** | 6.31 ± 0.046 | 6.13 ± 0.0858 | 6.10 ± 0.108 |
| **CM (V)** | 6.44 ± 0.114 | 6.30 ± 0.128 | 6.28 ± 0.136 |
| **TCM (s)** | 10.5 ± 2.36 | 15.0 ± 4.15 | 14.4 ± 3.25 |
| **CEP (V)** | 0.125 ± 0.090 | 0.163 ± 0.0718 | 0.188 ± 0.0828 |
| **QC** | 2 | 4 | 3 |
| **TS (s)** | 87.6 ± 51.6 | 317 ± 36.5 | 266 ± 17.7 |
| **TSS (s)** | 51.2 ± 54.1 | 33.1 ± 31.6 | 14.3 ± 5.09 |
| **%TiRPSS** | | 78.7% ± 20.3% | 86.3% ± 15.9% |
| **MEPSS (V)** | | 6.17 ± 0.0884 | 6.13 ± 0.110 |
| **VEPSS (V)** | | 4.62E-5 ± 7.52E-5 | 6.84E-5 ± 1.18E-4 |
| **SSEEPSS (V)** | | 0.0987 ± 0.152 | 0.0973 ± 0.164 |
| **%VAR(SI)** | | -0.132 ± 3.19 | -0.0138 ± 1.62 |
| **SMBF (ml/min/100g)** | | 0.362 ± 0.195 | 0.260 ± 0.163 |

**Table 1.** Summary of mean ± standard deviation for each measure collected.

There were no significant differences for C/DM in the T and P1/P2 groups. TSS improved from T/P1 to P1/P2, with $p = 0.31$ and 0.055, respectively. Removing the two most extreme outliers lowered these to $p = 0.17$ and 0.055 each (no change). For the other

performance measures (Figure 10), %TiRPSS did not have any significant relationships, but VEPSS had $p = 0.026$, and SSEEPS had $p$ 0.020 in C/DM, respectively.

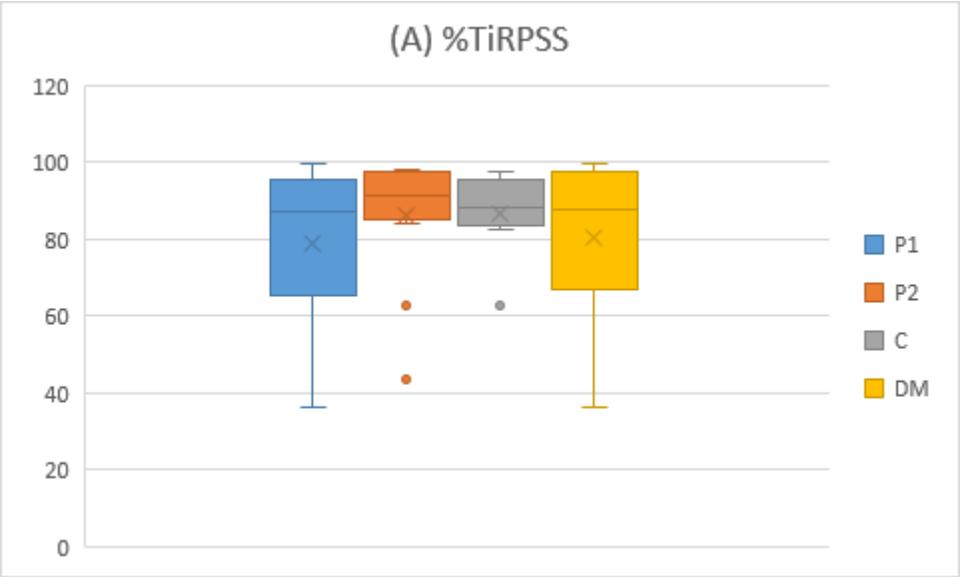


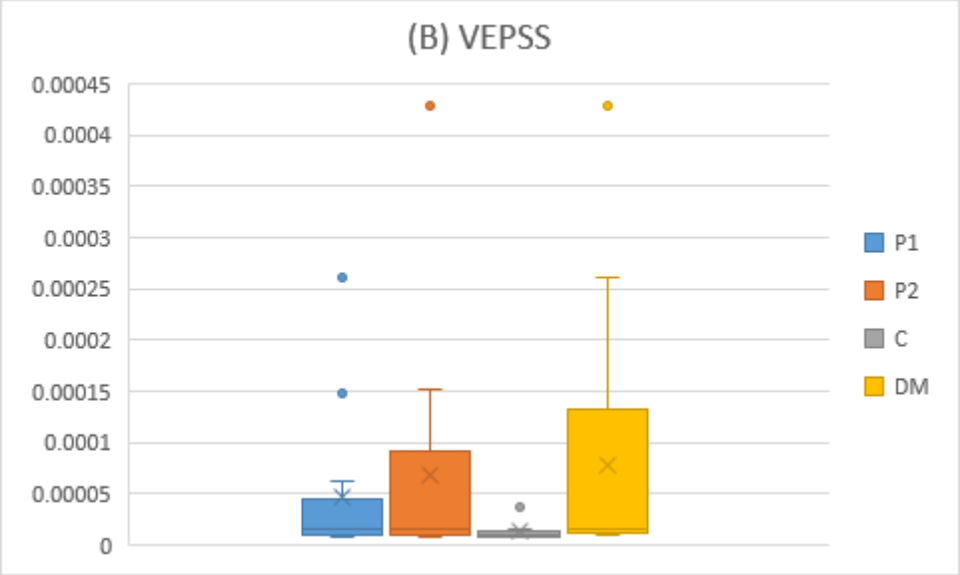

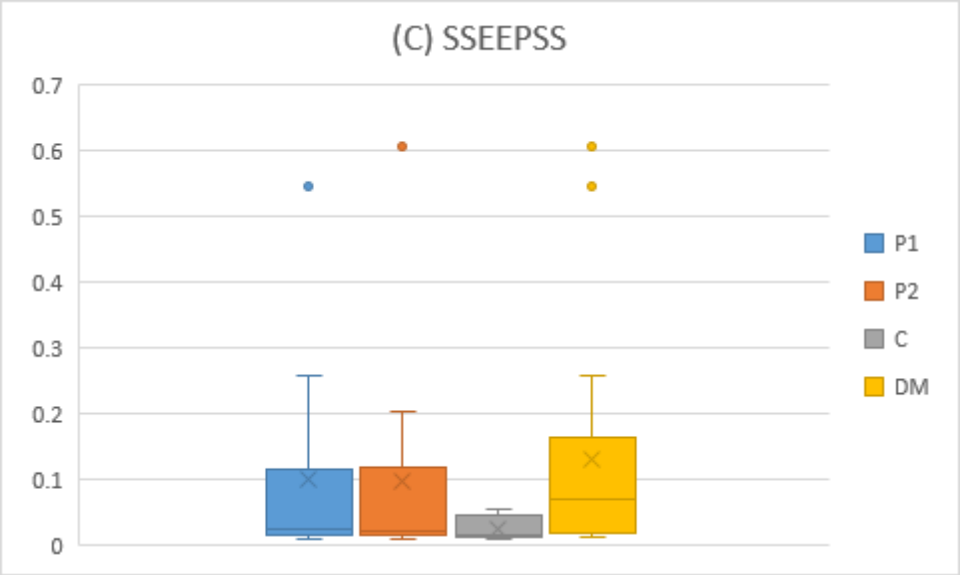


**Figure 10.** Boxplots of (A) %TiRPSS, (B) VEPSS, and (C) SSEEPSS) for P1/P2 and C/DM. Dots are outliers.

The regression of TEP vs. MEPSS had an $R^2$ of 0.97 (Figure 11).

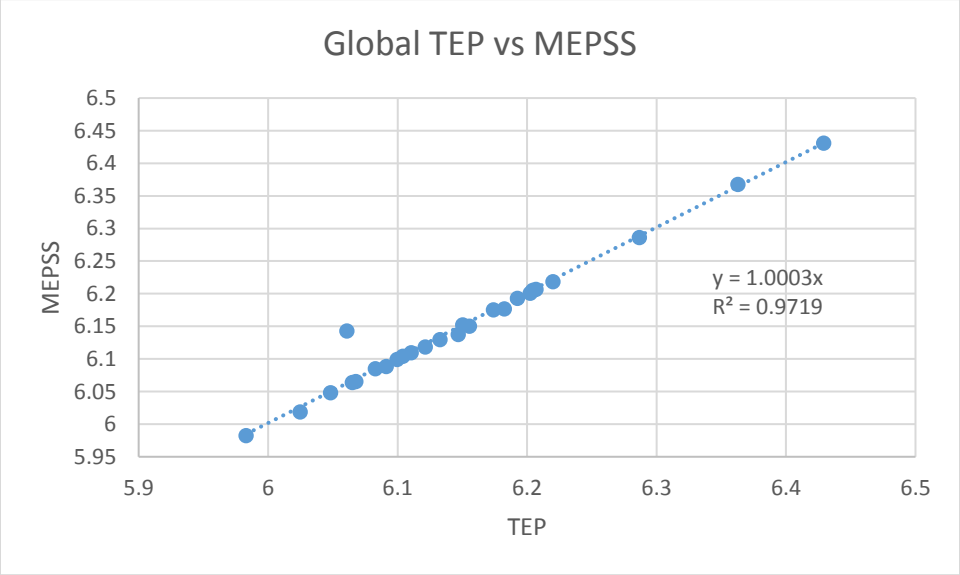


**Figure 11.** Plot of global TEP vs. MEPSS.

The correlations between calibration and subsequent scan performance were weak, and thus their plots were omitted. The two strongest correlations were CEP vs. VEPSS and CEP vs. SSEEPSS (Figure 12), with $R^2$ values of 0.31 and 0.30, respectively.

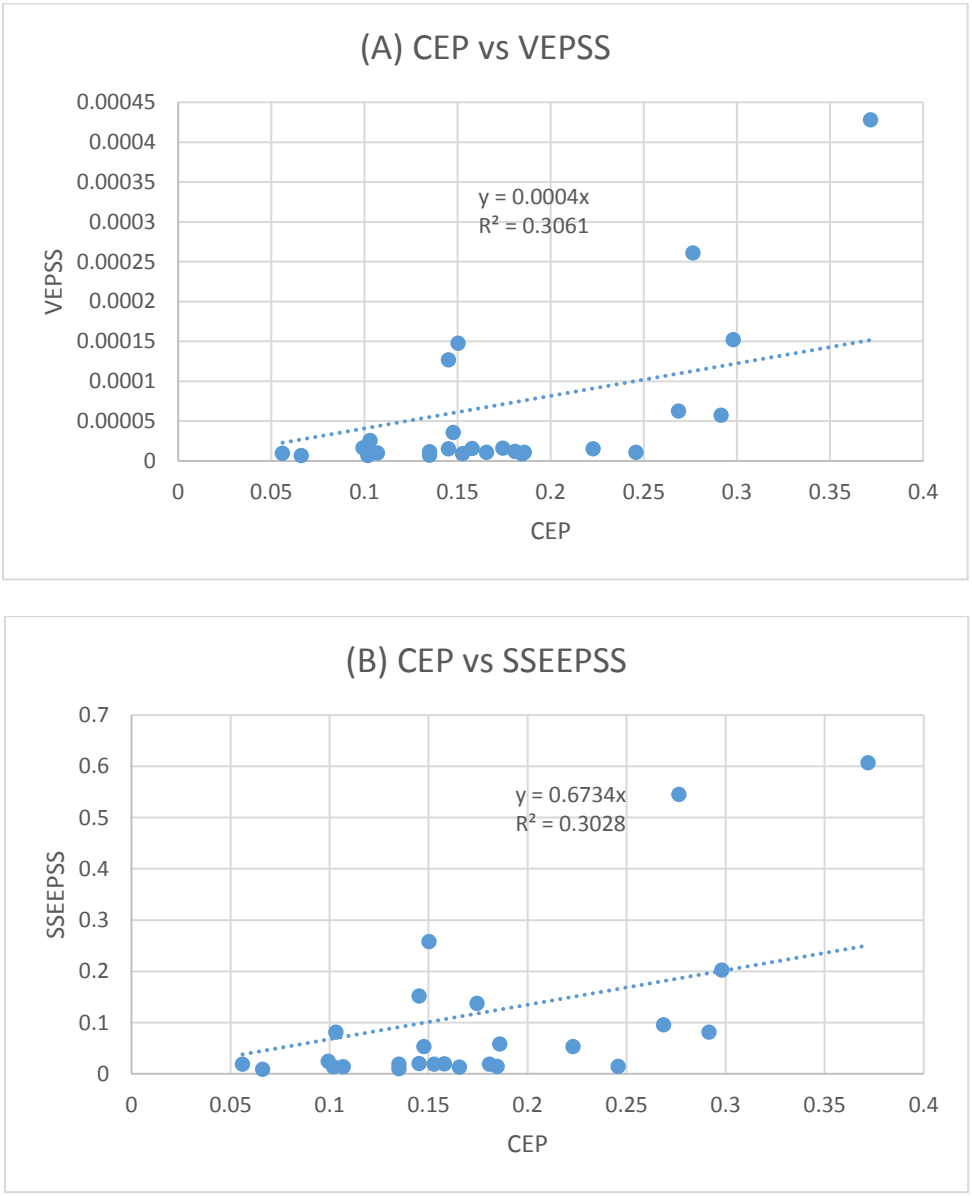


**Figure 12.** (A) Plot of CEP vs. VEPSS. (B) Plot of CEP vs. SSEEPSS.

There were several significant relationships found between QC and subsequent scan %TiRPSS, VEPSS, and SSEEPSS in the P1, P2, DM, and global sets (Figure 13 and Table 2).

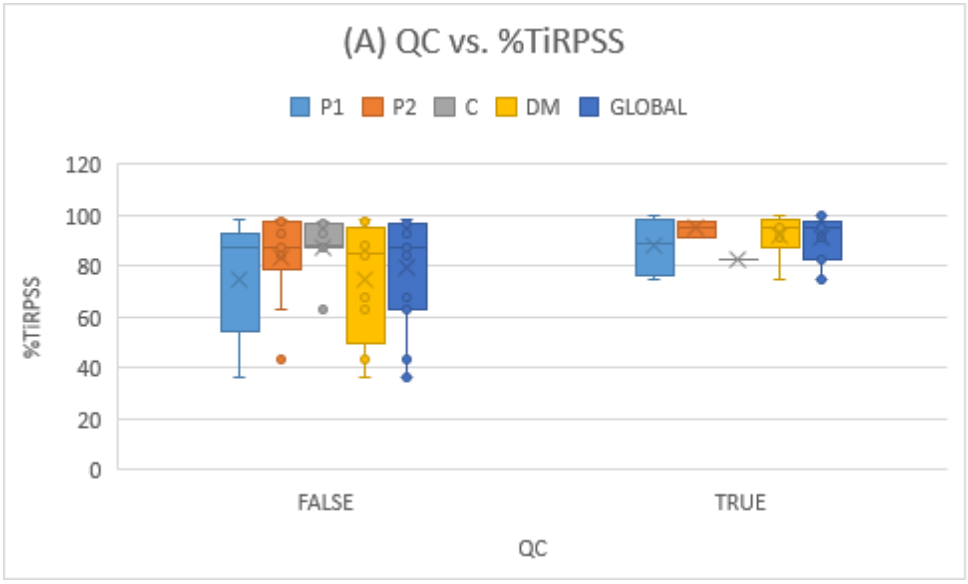


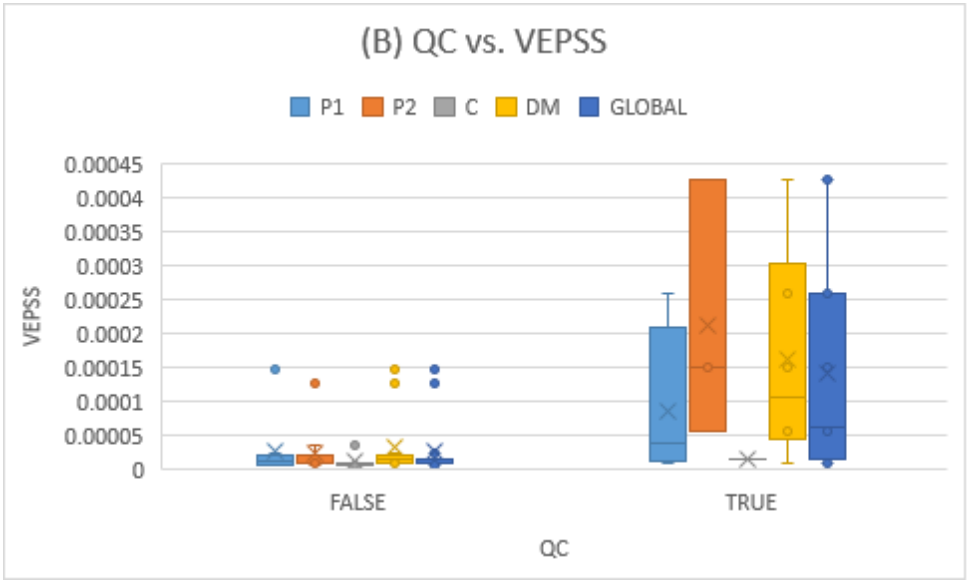

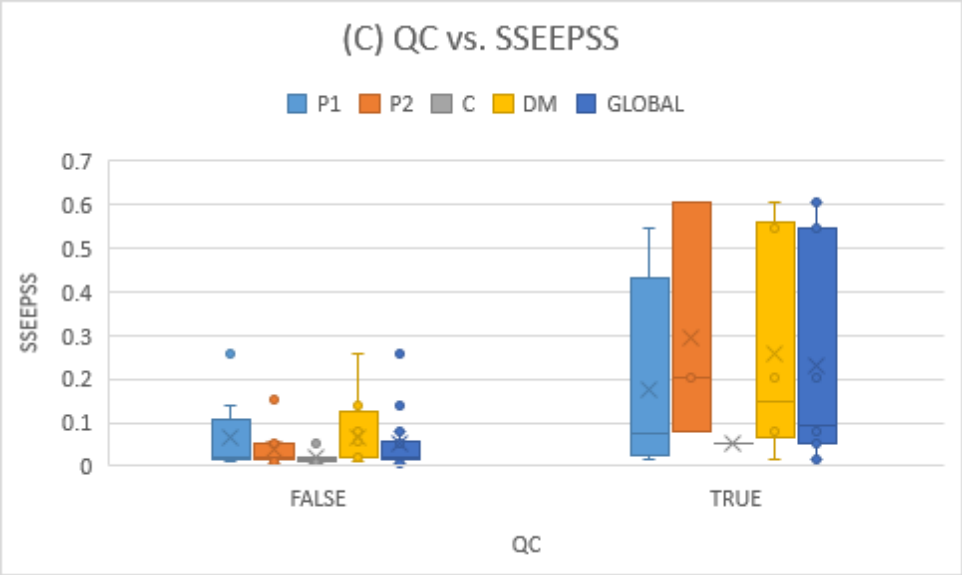


**Figure 13.** QC vs. %TiRPSS (A), vs. VEPSS (B), and vs. SSEEPSS (C).

| QC vs. | %TiRPSS | VEPSS | SSEEPSS |
|---|---|---|---|
| P1 | 0.19 | 0.39 | 0.43 |
| P2 | 0.081 | 0.23 | 0.24 |
| DM | 0.033 | 0.11 | 0.13 |
| GLOBAL | 0.058 | 0.098 | 0.10 |

**Table 2.** QC vs. %TiRPSS, VEPSS, and SSEEPSS, for P1, P2, DM, and global groups, *p*-values.

The correlations for T calibration measures vs. P1/P2 were weak and thus their plots were omitted. The only statistically significant *t* hypothesis tests were $p = 0.078$ for T QC vs. DM CEP, and $p = 0.041$ and 0.061 for T QC vs. the global set VEPSS and SSEEPSS, respectively (Figure 14). The most statistically significant $\chi^2$ result was $p = 0.14$ for T QC vs. C/DM QC.

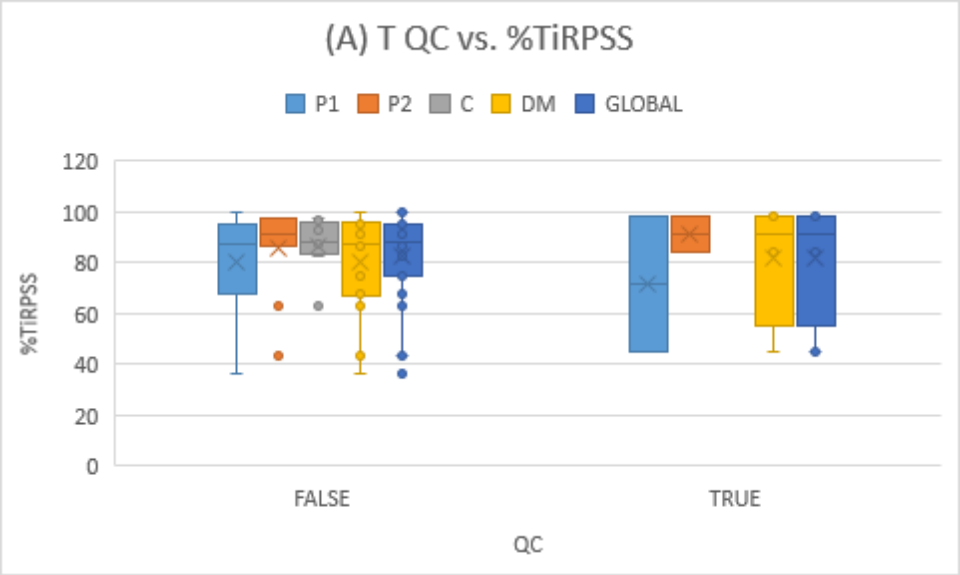
(A) T QC vs. %TiRPSS
P1
P2
C
DM
GLOBAL
120
100
80
60
40
20
0
%TiRPSS
FALSE
TRUE
QC

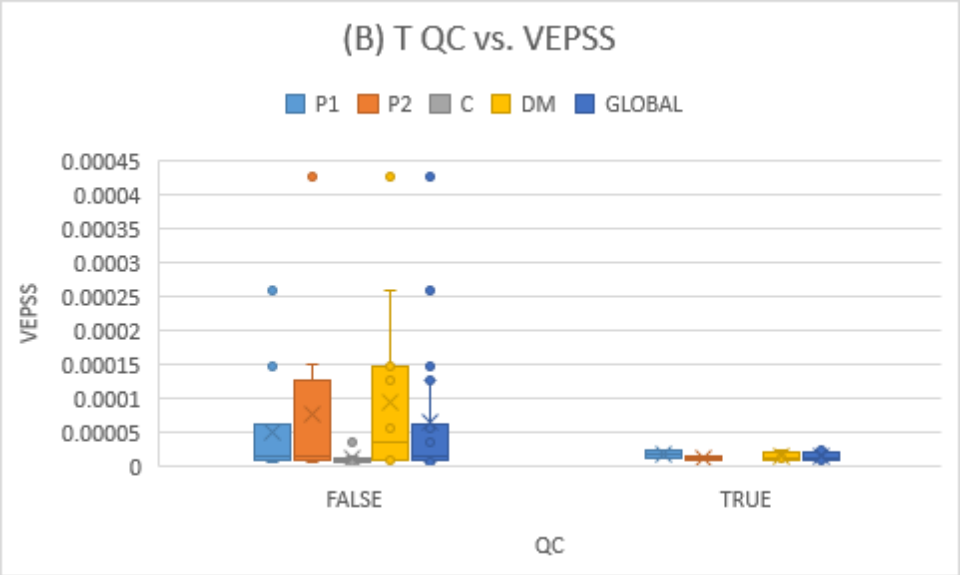
(B) T QC vs. VEPSS
P1
P2
C
DM
GLOBAL
0.00045
0.0004
0.00035
0.0003
0.00025
0.0002
0.00015
0.0001
0.00005
0
VEPSS
FALSE
TRUE
QC

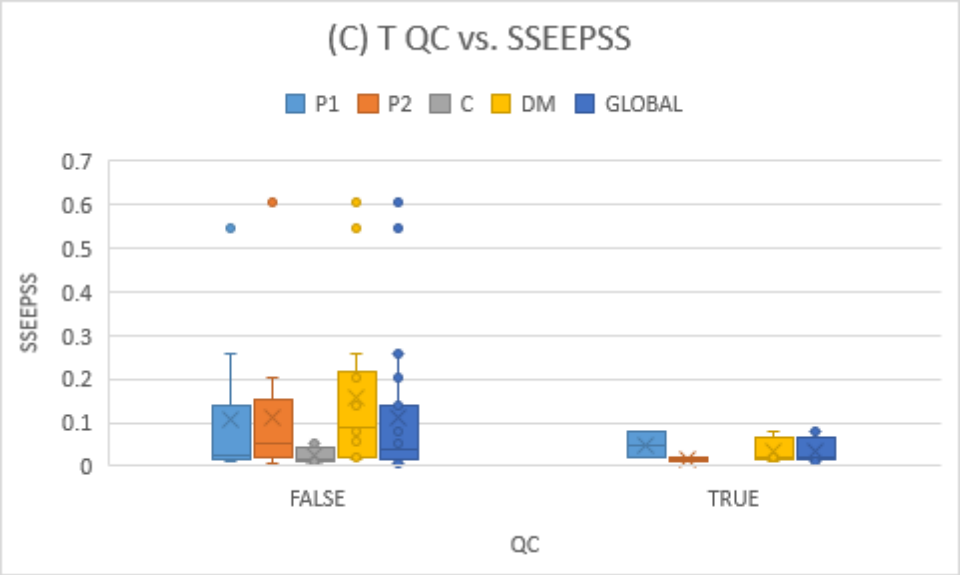


**Figure 14.** Boxplots T QC vs. %TiRPSS (A), VEPSS (B), and SSEEPSS (C) for P1, P2, C, DM, and global groups.

In our perfusion results, global P1/P2 SMBF was significantly elevated over that of R1/R2 at a $p = 0.0011$ level (Figure 15). Similarly, P1/P2 SMBF was significantly elevated over R1/R2 for both C and DM at $p = 0.044$ and 0.0094, respectively.

**Figure 15.** Boxplot of Rest vs. Stress SMBF.

There were no significant *t*-tests for global %VAR(SI). The timewise boxplot showed higher variance between rest and stress values, and their variance also trended up towards the end of the scan (Figure 16).

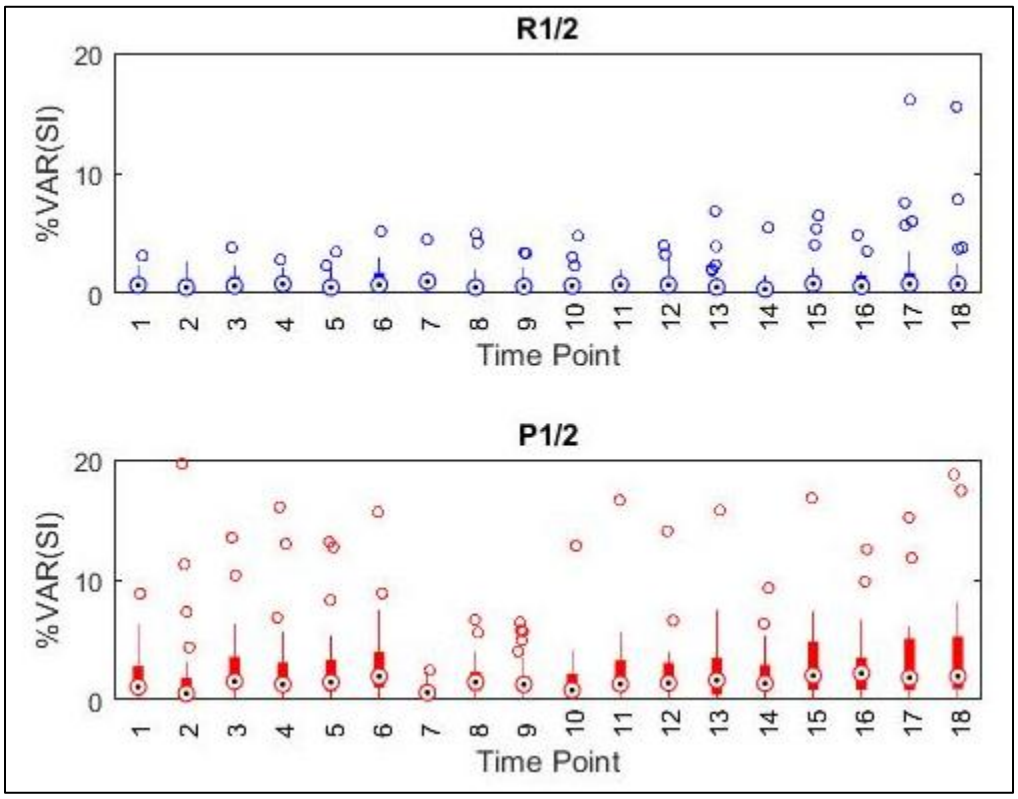


**Figure 16.** Timewise boxplot of %VAR(SI).

There were no significant correlations between the perfusion measures and performance measures, and thus these plots were omitted.

# 4. Discussion

## 4.1 Device Design

The pneumatic sensor proved to be an effective approach. The advantage of pneumatics was that they allow mechanical force to be measured while all electronic components to be well beyond the range of RF or B-field interference. In fact, this is a common approach in other MR compatible applications such as the emergency stop controls found in most scanner beds. A number of ideas for the pneumatic sensor were entertained, including a bladder with a hinged push panel, but ultimately the half-bulb design was settled on as the both most compatible with the desired muscle action and easiest to find commercially available components for.

Numerous improvements based on our clinical experience have been performed with the device. The photos in Figure 17A and 17B are annotated to point out some visible improvements to the foot assembly. The improvements' objectives were better biomechanical coupling, leak-proofing, signal filtering, and "quality-of-life" software and hardware improvements, like a newer-model laptop from which to control the device, dulled colors on the GUI to reduce subject eyestrain, and fully integrating the sensor coupling, gauge and fittings, and DAQ circuitry components into a single box.

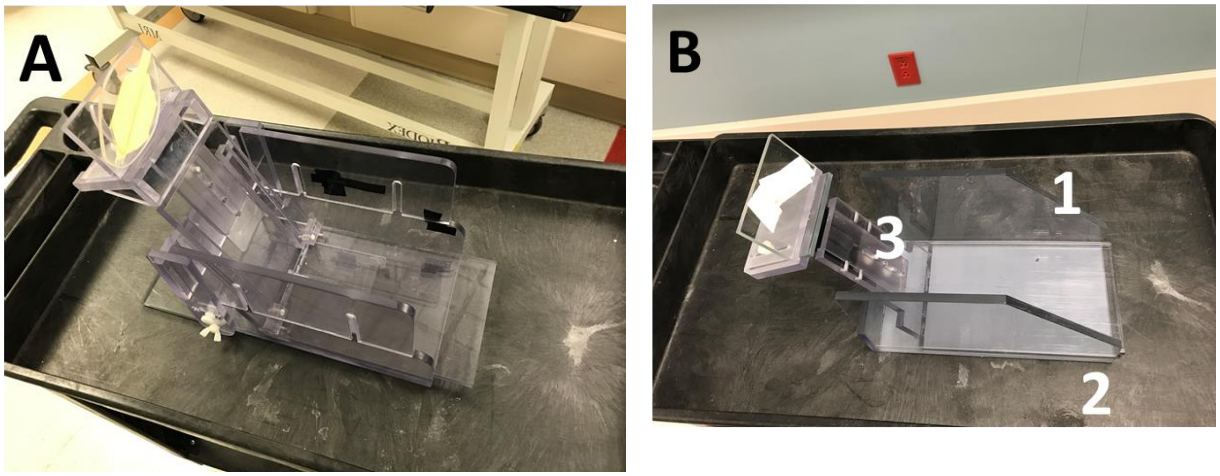


**Figure 17.** (A) Foot assembly, first iteration. (B) Foot assembly, second iteration. Point 1 shows the chamfered side panels to reduce profile. Point 2 is the slotted base to restrict the insert's vertical movement. Point 3 is the increased clearance between insert and side panels, to allow for better coil placement.

There are several remaining areas of potential improvement for the device. For starters, the gauge circuitry was made entirely with passive components. Active circuitry could help cut down on interference while magnifying the relevant pressure signal, which could further reduce the effect of system noise on the subject-display sensory feedback loop. Along those lines, other major components like the DAQ could potentially be replaced as well to improve overall efficiency. We did attempt to replace the bulb with a 3D-printed design, but the material was too weak and suffered blowouts.

Another major open issue was modeling the system's intrinsic leak rate. As was seen in Figure 16B, the absolute value of %VAR(SI) increased over time. One can intuitively understand that the leak rate should be proportional to the pressure in the system; when the subject pushes on the bulb, it increases the pressure and pushes air out of the system, which is closed and not being replenished because the small internal volume makes adjusting the inflow rate difficult.

Even if the system were being replenished, no inflow regulator could reactively respond in real time to the increased leak rate during stress.

As a result, we suspect that as the perfusion scan goes on, the growing leak rate forces the subject to exert more and more force, rather than achieving a constant level of exertion as would be desired. Indeed, we noted several subjects with our prototype who saw severe leaking and were unable to press hard enough to complete the 4-minute perfusion scans. After a comprehensive leak-proofing effort in our latest iteration of the pneumatic system, this was greatly reduced, but the system still leaks enough over any given 4-minute scan that the baseline pressure – the equilibrium measurement when the subject is not exerting any force at all – was often much lower after the scan than where it started.

Several attempts have been made to model this under first a Bernoulli model, and then an effusion model, neither of which could accurately explain the exponential-like decay seen in the voltage-time data from the validation experiment. We are currently consulting with one of the faculty of the chemistry department at our institution to find a solution to this problem. The ultimate goal would be to develop a model which would allow us to slowly adjust the display window downwards throughout each 4-minute scan based on an estimate of the additional amount of gas that has leaked due to the subject over that due to the intrinsic leak rate.

The last open question was how biomechanical coupling between the foot and the sensor bulb can be improved. The original version of the stage had the bulb mounted at an angle and

could adjust up or down to accommodate subjects with different foot lengths, but this allowed the subject to arch their entire foot, exerting their calf muscles, instead of forcing them to curl their toes and exert the digital flexor muscles in the sole of the foot, as desired. The solution to this, a tarsal curl bar and some restraining straps, have had some success, but introduced a new problem: because the toes are oriented diagonally, not every toe can curl around the bar. As yet we have been unable to devise a solution that can maintain the system's ambipedal flexibility and allow for rotation of the curl bar to accommodate the incline of the subject's toe line.

## 4.2 Statistical Analysis

The experimentally determined pressure-voltage curve boasted the most significant correlation coefficient of this entire research project. This result also agreed with the manufacturer's specifications.

The evaluation study was a small sample size, which likely reduced the power in finding relationships between the various measures studied. Also because of this, it was not possible to examine age, gender, or racial differences in the subject set. This was not likely to be a confounding factor in training or performance measures, but epidemiologically-driven racial differences and gender dimorphisms in the general subject population may play some small part in stress testing response. A much larger, racially- and gender-representative study would be able to rule out these unlikely factors, but at this stage of development, the cost would not be justified. Each of the measures used in the statistical analysis was chosen because it could describe a specific aspect of the acquisition. For instance, TEP-MEPSS and SSEEPSS measured how well

the subject matched the target on average, and VEPSS measured the subject's ability to maintain a stable pressure regardless of the actual mean pressure level, while %TiRPSS measured how well the subject stayed in the target range. TCM indicated how long it took for the subject to achieve their calibrated maximum, a potential measure of performance. QC was a discretized version of CEP, both measuring the quality of a calibration. TSS was a potential performance measure of training efficiency and subject learning ability – presumably, the more practice a subject got, the less time they would initially need to achieve stable stress. Lastly, %VAR(SI) was somewhat a measure of movement, though not entirely, since variance could increase due to subject exertion, and SMBF was a direct measure of perfusion, though sometimes a highly variable one between subjects and measurements – because it was calculated through a nonlinear regression, such an algorithm is vulnerable to false minima.

An interesting note was that the number of successful calibrations on the first try, NFC, which was mentioned earlier but not included for analysis, consecutively increased between the training (T) and each stress (P1/P2) scan, but the relationship was not statistically significant. Similarly, another way of describing this was that the average number of calibrations per scan steadily reduced between each group. However, this was not further explored because of the limited data and thus limited statistical significance.

Curiously, the reported averages for TSS would lead one to believe that a statistically significant relationship could easily be found for both T vs. P1 and P1 vs. P2. However, even

without outliers, T vs. P1 was not as significant as its counterpart. A larger sample and more stringent training protocols might further illuminate this phenomenon.

Of the relationships between the C and DM groups for T and P1/P2, none were statistically significant at the $p = 0.05$ level. A few, including P1 %TiRPSS and P2 CEP, were close to the $p = 0.10$ level, but could not be repeated in their counterpart group (P2 and P1, respectively). The most significant relationships for *both* P1 and P2 were for VEPSS and SSEEPSS. This may reflect better muscle control among the control subjects than the DM ones. This was reinforced by the even more significant global C/DM *p*-values, both near the $p = 0.025$ threshold.

As Figure 11 showed, global TEP vs. MEPSS had a very high correlation with only a single outlier that was likely due to either a study failure or a tabulation error that was overlooked in the analysis stage. This result, paired with our VEPSS and SSEEPSS findings and anecdotal observations, suggests that subjects overall did a good job of staying within the target range. The relationships between CEP/VEPSS and CEP/SSEEPSS were very notable; since they are so similar, this was very surprising. However, the upward trend between CEP and these two was notable. A commensurate increase in variance and error to the increase in CEP should be expected, since CEP determines both the TEP and the scale of the target range. But instead there was a flatter trend, which suggests that subject accuracy does increase with the CEP. This agrees with our experimental observation that the effect of the remaining inherent noise in the DAQ signal on the subject-display feedback loop was lessened at higher CEP because it directly

determined the vertical limits of the interactive display axes, reducing their contribution to the subject's visual distraction. Similarly, the link between QC and %TiRPSS, VEPSS, and SSEEPSS likely captured some of this effect, as well as showing some justification for our observed link between QC and overall performance; many of the *p*-values (Table 3) were statistically significant at the 0.1 level and below. Given the paucity of quality calibrations, however, we believe this merits further study before enshrinement as a golden standard.

Unfortunately, while some more superficial training measures like NC, NFC, and TSS reduced with each consecutive acquisition, none of the training measures could reliably predict later performance, with the exception again of QC and its partners VEPSS and SSEEPSS. While the global result was strong, the lack of relationship with CEP suggests that this could potentially be spurious nonetheless, though this is still an unlikelihood.

In looking at our perfusion measures, a significant difference was only found between rest and stress, both globally and between the C and DM groups. This was somewhat surprising, as the strong relationships between calibration and VEPSS and SSEEPSS suggested that they might be reactive to %VAR(SI); instead, the weak correlations to %VAR(SI), which as mentioned was primarily a measure of in-scan movement, leads us to the hypothesis that the majority of SMBF influence on VEPSS and SSEEPSS was due to actual changes in perfusion, not movement. This would be good news, since it would mean that perfusion can be measured over moderate periods of time without image quality suffering due to the inherent instability of

muscle control in older subjects and those with impaired neural foot muscle control, two features of the DM and ulcer patient populations.

There are several limitations in this study. First, a larger sample size would be needed to resolve some of the open analysis questions and zero in on other potential relationships. More advanced statistical measures could also influence design directions by illuminating areas for improvement. The device itself could be further refined with better leak sealing, biomechanical coupling, comfort and ergonomics, and more sensitive circuitry, possibly involving active electronics – along with the protocol modifications these features would necessitate. Lastly, as mentioned we are currently working on a leakage model to correct the most serious issue with the current prototype in achieving a stable sensory feedback loop to ensure consistent stress.

Finally, the absolute value boxplots for %VAR(SI) suffered from numerous outliers, but the key takeaway was that it was much higher for stress vs. rest. It is possible, though unlikely in light of the above discussion, that this could be due to in-scan motion. If so, these could be mitigated by a better-designed restraint system as well as a stricter training and stress acquisition protocol.

# 5. Conclusion

In conclusion, we have achieved our goal of building an MR-compatible pneumatic sensor device to create a sensory feedback loop for consistent foot perfusion stress testing. The device itself was very economical to build, and relied on widely available materials. The linearity

of the device's pressure-voltage correlation was validated and a working protocol was developed, with minimal setup required. This prototype could pave the way towards a clinically viable solution for MR foot perfusion stress testing, and its principle could even be expanded to other applications in the broader fields of imaging and stress testing.

# References


1. "Statistics About Diabetes." American Diabetes Association, 2017. URL: http://www.diabetes.org/diabetes-basics/statistics/
2. ME Mitchell. "Lower Extremity Major Amputations." In: AN Sidaway (ed). "Diabetic Foot: Lower Extremity Arterial Disease and Limb Salvage." Philadelphia: Lippincott Williams & Wilkins, 2006; 341-50.
3. C Grunfeld. "Diabetic foot ulcers: etiology, treatment and prevention." Adv Intern Med, 1992; 37:103–32.
4. ME Edmonds, AVM Foster. "Managing the Diabetic Foot." Blackwell Science Press, 2000.
5. T Dinh, A Veves. "Microcirculation of the Diabetic Foot." Curr Pharm Des, 2005; 11:2301–9.
6. RA Malik, PG Newrick, AK Sharma, A Jennings, AK Ah-See, TM Mayhew, J Jakubowski, AJ Boulton, JD Ward. "Microangiopathy in Human Diabetic Neuropathy: Relationship Between Capillary Abnormalities and the Severity of Neuropathy." Diabetologia, 1989; 32:92-102.
7. FW LoGerfo, JD Coffman. "Current Concepts. Vascular and Microvascular Disease of the Foot in Diabetes. Implications for Foot Care." N Engl J Med, 1984; 311:1615-9.
8. KA Arsenault, J McDonald, PJ Devereaux, K Thorlund, JG Tittley, RP Whitlock. "The use of Transcutaneous Oximetry to Predict Complications of Chronic Wound Healing: A Systematic Review and Meta-Analysis." Wound Repair Regen, 2011; 19:657–63.

9. A Challoner. “Photoelectric Plethysmography for Estimating Cutaneous Blood Flow.” In: P Rolfe (ed). “Non-Invasive Physiological Measurement.” London: Academic Press, 1979; 125–51.
10. CI Wright, CI Kroner, R Draijer. “Non-invasive Methods and Stimuli for Evaluating the Skin’s Microcirculation.” J Pharmacol Toxicol Methods 2006; 54:1–25.
11. AC Shore. “Capillaroscopy and the Measurement of Capillary Pressure.” Br J Clin Pharmacol, 2000; 50:501–13.
12. GB Yvonne-Tee, AH Rasool, AS Halim, AR Rahman. “Noninvasive Assessment of Cutaneous Vascular Function in vivo using Capillaroscopy, Plethysmography and Laser-Doppler Instruments: Its Strengths and Weaknesses.” Clin Hemorheol Microcirc, 2006; 34:457–73.
13. RE Pecoraro, JH Ahroni, EJ Boyko, VL Stensel. “Chronology and Determinants of Tissue Repair in Diabetic Lower-Extremity Ulcers.” Diabetes, 1991; 40:1305-13.
14. B Fagrell. “Peripheral Vascular Disease.” In: AP Shepherd, AA Oberg (eds). “Laser: Doppler Flowmetry” Kluwer Academic Publishers, Boston, 1990; 201–14.
15. A Humeau, W Steenbergen, H Nilsson, T Stromberg. “Laser Doppler Perfusion Monitoring and Imaging: Novel Approaches.” Med Biol Eng Comput, 2007; 45:421–35.
16. J Cobb, D Claremont. “Noninvasive Measurement Techniques for Monitoring of Microvascular Function in the Diabetic Foot.” Int J Low Extrem Wounds, 2002; 1:161–9.
17. JJ Jr Castronuovo, HM Adera, JM Smiell, RM Price. “Skin Perfusion Pressure Measurement is Valuable in the Diagnosis of Critical Limb Ischemia.” J Vasc Surg, 1997; 26:629-37.

18. W Groner, JW Winkelman, AG Harris, et al. “Orthogonal Polarization Spectral Imaging: A New Method for Study of the Microcirculation.” Nat Med, 1999; 5:1209–12.
19. CYL Chao, GLY Cheing. “Microvascular Dysfunction in Diabetic Foot Disease and Ulceration.” Diabetes Metabolism Res Rev, 2009; 25:604 –14.
20. EJ Boyko, JH Ahroni, VL Stensel, DG Smith, DR Davignon, RE Pecoraro. “Predictors of Transcutaneous Oxygen Tension in the Lower Limbs of Diabetic Subjects.” Diabet Med, 1996; 13:549–54.
21. E Faglia, G Clerici, M Caminiti, A Quarantiello, V Curci, A Morabito. “Predictive Values of Transcutaneous Oxygen Tension for Above-the-Ankle Amputation in Diabetic Patients with Critical Limb Ischemia.” Eur J Vasc Endovasc Surg, 2007; 33:731–6.
22. D Yudovsky, A Nouvong, K Schomacker, L Pilon. “Monitoring Temporal Development and Healing of Diabetic Foot Ulceration Using Hyperspectral Imaging.” J Biophotonics, 2011; 4:565-76.
23. ST Krishnan, NR Baker, AL Carrington, G Rayman. “Comparative Roles of Microvascular and Nerve Function in Foot Ulceration in Type 2 Diabetes.” Diabetes Care, 2004; 27:1343-8.
24. KT Moriarty, AC Perkins, AM Robinson, ML Wastie, RB Tattersall. “Investigating the Capillary Circulation of the Foot with $^{99m}$Tc-Macroaggregated Albumin: A Prospective Study in Patients with Diabetes and Foot Ulceration.” Diabet Med, 1994; 11:22-7.
25. RL Greenman, S Panasyuk, X Wang, TE Lyons, T Dinh, L Longoria, JM Giurini, J Freeman, L Khaodhiar, A Veves. “Early Changes in the Skin Microcirculation and Muscle Metabolism of the Diabetic Foot.” Lancet, 2005; 366:1711-7.

26. J Zheng, H An, A Coggan, X Zhang, A Bashir, D Muccigrosso, L Peterson, R Gropler. "Noncontrast Skeletal Muscle Oximetry." Magnetic Resonance in Medicine, Jan 2014; 71(1):318-25. doi: 10.1002/mrm.24669. Epub 2013 Feb 19.

27. D Muccigrosso, X He, D Abendschein, A Bashir, W Chen, RJ Gropler, J Zheng. "Methods for Quantification of Absolute Myocardial Oxygen Consumption with O17 MRI." Oral Presentation, *ISMRM Annual Meeting, 2011*.

28. J Zheng, MK Hasting, X Zhang, A Coggan, H An, D Muccigrosso, D Snozek, A Bashir, RJ Gropler, J Curci, MJ Mueller. "Regional Perfusion and Oxygenation in Calf Muscles are Attenuated in Diabetes." J Vasc Surg, 2014; 59:419-26.

29. J Zheng, MK Hastings, D Muccigrosso, ZY Fan, J Curci, CF Hildebolt, MJ Mueller. "Non-contrast MRI Perfusion Angiosome in Diabetic Feet." European Radiology, 2015; 25:99-105.